Muon Pair Production by Electron-Photon Scatterings

H. Athar[1,2,*], Guey-Lin Lin[2,†] and Jie-Jun Tseng[2,‡]

[1] *Physics Division, National Center for Theoretical Sciences, Hsinchu 300, Taiwan*

[2] *Institute of Physics, National Chiao Tung University, Hsinchu 300, Taiwan*

(February 1, 2008)

The cross section for muon pair productions by electrons scattering over photons, σ_{MPP}, is calculated analytically in the leading order. It is pointed out that for the center-of-mass energy range, $s \geq 5\,m_\mu^2$, the cross section, σ_{MPP} is less than $1\,\mu$b. The differential energy spectrum for either of the resulting muons is given for the purpose of high-energy neutrino astronomy. An implication of our result for a recent suggestion concerning the high-energy cosmic neutrino generation through this muon pair is discussed.

PACS number(s): 12.15.Ji, 13.90.+i, 11.80.Gw, 14.60.Ef

High-energy neutrino astronomy is now a rapidly developing field [1]. This entails the identification of possible sources for high-energy cosmic neutrinos. In particular, non hadronic processes taking place in cosmos remain an interesting possible source for high-energy neutrinos.

In this context, Kusenko and Postma have recently suggested that, for a class of topological defects that may produce ultrahigh-energy photons at high red shift, the dominance of muon pair production (MPP) in $e^-\gamma \to e^-\mu^+\mu^-$ over triplet pair production (TPP) in $e^-\gamma \to e^-e^+e^-$ for $s \geq 5\,m_\mu^2$ enables the MPP process to be an efficient mechanism for generating high-energy cosmic neutrinos [2]. The electrons in the initial state of the above processes are considered as originating from the electromagnetic cascade generated by the ultrahigh-energy photons scattering over the cosmic microwave background photons present at high red shift. Subsequently, assuming that this ultrahigh-energy photon source at high red shift is responsible for the observed flux of ultrahigh-energy cosmic rays, it was pointed out that the decays of muons in MPP give rise to high-energy cosmic neutrino flux $E_\nu^2\phi_\nu$ typically peaking at $E_\nu \sim 10^{17}$ eV [3]. Concerning the cross sections of the above processes, we note that, although TPP process has been thoroughly studied before

*E-mail: athar@phys.cts.nthu.edu.tw

†E-mail: glin@cc.nctu.edu.tw

‡E-mail: geny.py86g@nctu.edu.tw

[4], there is still no explicit estimate for σ_{MPP} for $s \geq 5\,m_\mu^2$ to our knowledge. In order to verify whether MPP indeed dominates over TPP for $s \geq 5\,m_\mu^2$, we analytically calculate the σ_{MPP} for $5\,m_\mu^2 \leq s \leq 20\,m_\mu^2$. In this *Rapid Communication*, we present some details of the calculation and compare our result with the value quoted in Refs. [2,3]. Our conclusion is that, within the above s range, the cross section σ_{MPP} we have obtained is at least three orders of magnitude smaller than the one quoted and used in Refs. [2,3]. This implies that MPP can not be the dominating high-energy neutrino generating process as suggested in Refs. [2,3]. This conclusion is based upon the value of the ratio R defined as $R \simeq \sigma_{MPP}/(\eta_{TPP}\sigma_{TPP})$ [2], where $\eta_{TPP}(s) \simeq 1.768(s/m_e^2)^{-0.75}$ is the inelasticity for TPP and $\sigma_{TPP} \simeq \alpha^3 m_e^{-2}\,[3.11\ln(s/m_e^2) - 8.07]$, both for $s \gg m_e^2$ [4]. The η_{TPP} is basically the average fraction of the incident energy carried by the final state positron. The original estimate of Refs. [2,3] gives $R \simeq 10^2$, which favors MPP process as the dominating cosmic high-energy neutrino generating process. Namely the electron energy attenuation length due to TPP process is much longer than the interaction length of MPP process. However, since the correct value for σ_{MPP} within the energy range $5\,m_\mu^2 \leq s \leq 20\,m_\mu^2$ is three orders of magnitude smaller, the ratio R becomes less than 1. Therefore MPP is no longer an effective mechanism for generating high-energy cosmic neutrinos at the high red shift.

There are 8 Feynman diagrams contributing to the MPP process in the leading order. These are shown in Fig. 1. Among these 8 diagrams, 4 diagrams contain a Z-boson exchange, which can be disregarded for the range of s under discussion. Among the remaining 4 diagrams, one can also disregard diagrams (c) and (d) due to the inflow of large invariant energies into the electron [diagram (c)] or photon [diagram (d)] propagators. We therefore only perform analytic calculations for diagrams (a) and (b) in Fig. 1 while evaluate the rest of the diagrams numerically. We have applied the equivalent photon approximation [5] to compute diagrams (a) and (b). We write the MPP cross section in the following convolution

$$\sigma_{MPP} = \int_{4m_\mu^2/s}^{1} dx f_{\gamma/e}(x)\sigma_{\gamma\gamma\to\mu^+\mu^-}(\hat{s} = xs), \tag{1}$$

where $f_{\gamma/e}(x) = (\alpha/2\pi)[(1+(1-x)^2)/x]\ln(s/m_e^2)$ is the probability of finding a photon from the incident electron with an energy fraction $x = E_\gamma/E_e$. The differential cross section as a function of the outgoing muon energy E_μ, in head on collisions, is given by

$$\begin{aligned}\frac{\mathrm{d}\sigma_{MPP}}{\mathrm{d}y} \simeq{}& \frac{\alpha^3}{m_\mu^2 y}\left[1+\left(1-\frac{4m_\mu^2y^2}{s}\right)^2\right]\ln\left(\frac{s}{m_e^2}\right)\\ &\times(1-v^2)\left[\left(1+\frac{1}{y^2}\right)\ln\left(\frac{1+v}{1-v}\right) - v - \frac{1}{y^4}\left(\frac{v}{1-v}+\tanh^{-1}(v)\right)\right],\end{aligned} \tag{2}$$

where $y = E_\mu/m_\mu$ with $y_{min} = 1$ and $y_{max} = \sqrt{s}/2m_\mu$; v is the velocity of the outgoing muon, which is related to y by $v = \sqrt{1-\frac{1}{y^2}}$. Apart from the trivial prefactor, the first line in Eq. (2) arises from the distribution function $f_{\gamma/e}(x)$ while the second line describes the cross section

for $\gamma\gamma \to \mu^+\mu^-$. The total cross section σ_{MPP}, obtained by performing the y integration, depends only on the center-of-mass energy $\sqrt{s}$. For $s = 5\,m_\mu^2$, $\sigma_{MPP} \simeq 4 \cdot 10^{-3}\,\mu$b, while σ_{MPP} increases to about $0.1\,\mu$b for $s = 20\,m_\mu^2$. These cross-section values are at least 3 orders of magnitudes smaller than those of Refs. [2,3], which give σ_{MPP} between 0.1 and 1 mb in the above energy range. The last equation gives the differential energy spectrum of either of the muons produced in MPP. In the large s limit, the σ_{MPP} given by Eq. (2) behaves as

$$\sigma_{MPP}(s) \simeq \frac{2\alpha^3}{m_\mu^2} \ln(2) \ln\left(\frac{s}{m_e^2}\right). \tag{3}$$

The inelasticity for MPP (in the center-of-mass frame) is defined as

$$\eta_{MPP}(s) = \frac{1}{\sigma_{MPP}(s)} \int dE_\mu \left(\frac{E_\mu}{\sqrt{s}}\right) \frac{d\sigma_{MPP}}{dE_\mu}. \tag{4}$$

Using Eqs. (2) and (4), we find that the average fraction of incident energy carried by either of the muons in MPP, in the large s limit, behaves as

$$\eta_{MPP}(s) \simeq 3.44 \left(\frac{s}{m_\mu^2}\right)^{-0.5}, \tag{5}$$

whereas it is close to 0.48 near the threshold for the MPP process and approaches to 0.34 for $s \sim 20\,m_\mu^2$.

We have used a package for computations in high energy physics, CompHEP (version 33.22), to check our results for σ_{MPP} [6]. The comparison for $5\,m_\mu^2 \le s \le 20\,m_\mu^2$ is shown in Fig. 2. We note that the plot generated by CompHEP is a result of computing all 8 diagrams. From Eq. (2), we also note that, for $s \gg 5\,m_\mu^2$, the MPP cross section $\sigma_{MPP} < 1\,\mu$b. We have confirmed this remark using CompHEP as well. We have made a further check on our σ_{MPP} by generating the amplitude of diagrams (a) and (b) symbolically using the package *FeynArts* 3 [7]. In this procedure, we do not use the equivalent photon approximation. We then obtained σ_{MPP} by numerically performing the phase space integration. We have found a rather good agreement (within few percent) between the σ_{MPP} obtained in this way and that given by the equivalent photon approximation. Because of the rather lengthy algebraic expressions occurring in the above procedure, we are omitting further details of this check.

To obtain a consistent estimate of R, it is desirable to compute σ_{TPP} and η_{TPP} in addition to σ_{MPP}. This can be easily done in the large s limit. By replacing $\mu^\pm$ with $e^\pm$ in the final state, the same 8 diagrams shown in Fig. 1 also contribute to the TPP process in the leading order. The dominating diagrams are again the first two. In the equivalent photon approximation with $s \gg m_e^2$, they give

$$\sigma_{TPP}(s) \simeq \frac{\alpha^3}{m_e^2} \ln(2) \ln\left(\frac{s}{m_e^2}\right), \tag{6}$$

whereas

$$\eta_{TPP}(s) \simeq 3.44 \left(\frac{s}{m_e^2}\right)^{-0.5} . \tag{7}$$

The result for σ_{TPP} can be easily inferred from Eq. (3) by replacing m_μ^2 there with m_e^2 and multiplying a symmetry factor 1/2 which takes into account the identical-particle effect in the TPP process. The above results for σ_{TPP} and η_{TPP} agree well (within few percent) with the results quoted in [4]. We further evaluated $\eta_{TPP}(s)$ in the Lab frame also, which in the large s limit, for the two dominating diagrams, is $\sim 0.25(s/m_e^2)^{-0.5}$. In practice, one should use the Lab-frame η_{TPP} in the the definition of R. Numerically, the Lab-frame η_{TPP} is approximately an order of magnitude smaller than its center-of-frame counterpart. This suppression is related to the kinematical factors present in the Lorentz boost from the center-of-mass frame to the Lab-frame. Using the Lab-frame η_{TPP} and the values for σ_{TPP} and σ_{MPP}, we still obtain $R < 1$ for $5\,m_\mu^2 \leq s \leq 20\,m_\mu^2$.

In summary, the authors in Refs. [2,3] use the value 0.1-1 mb for the cross section σ_{MPP} in the energy range $5\,m_\mu^2 \leq s \leq 20\,m_\mu^2$. As a result, they have deduced that $R \simeq \sigma_{MPP}/(\eta_{TPP}\sigma_{TPP}) \gg 1$. However, as we have shown, the correct value for σ_{MPP} obtained from Eq. (2) yields $R < 1$. In particular, near the threshold for the MPP process, i.e., for $s \sim 5\,m_\mu^2$, we have $R \ll 1$. Therefore, based on this observation, we conclude that MPP can not be a dominating high-energy cosmic neutrino generating process as suggested in Refs. [2,3]. Furthermore, we have also derived analytic expressions (in the leading order) for differential energy spectrum and the inelasticity of the MPP process in the large s limit, which might be of relevance in some other contexts of high-energy neutrino astronomy.

For completeness, let us add a final remark concerning the possibility of high-energy cosmic neutrino generation in an electromagnetic cascade at high red shift, z, through $\gamma\gamma$ collisions. The process $\gamma\gamma \to \mu^+\mu^-$ can, in principle, generate high-energy cosmic neutrinos near the threshold for this process, namely, for $\sqrt{s} \simeq 2\,m_\mu$. The neutrinos are generated through the subsequent decays of the final-state muons for a rather small range of z values, typically, for $z \sim 5-10$. In this z range, the interaction length for the process $\gamma\gamma \to \mu^+\mu^-$ is smaller than the energy attenuation length dictated by the process $\gamma\gamma \to e^+e^-$. Furthermore, this interaction length is also smaller than the horizon length, $cH(z)^{-1}$, where $H(z)$ is the Hubble constant in this z range.

ACKNOWLEDGMENTS

HA thanks Physics Division of NCTS for financial support. GLL and JJT are supported by the National Science Council of R.O.C. under the grant number NSC89-2112-M009-041.

[1] For some recent discussions, see, for instance, D. B. Cline and F. W. Stecker, astro-ph/0003459; H. Athar, hep-ph/0008121; R. Gandhi, Nucl. Phys. Proc. Suppl. **91**, 453 (2001) [hep-ph/0011176]; T. K. Gaisser, astro-ph/0011525.

[2] A. Kusenko and M. Postma, Phys. Rev. Lett. **86**, 1430 (2001) [hep-ph/0007246].

[3] M. Postma, Phys. Rev. D **64**, 023001 (2001) [hep-ph/0102106].

[4] V. Anguelov, S. Petrov, L. Gurdev and J. Kourtev, J. Phys. G **25**, 1733 (1999) [astro-ph/0001252], and references cited therein.

[5] S. J. Brodsky, T. Kinoshita and H. Terazawa, Phys. Rev. D **4**, 1532 (1971).

[6] A. Pukhov *et al.*, hep-ph/9908288.

[7] T. Hahn, hep-ph/0012260.

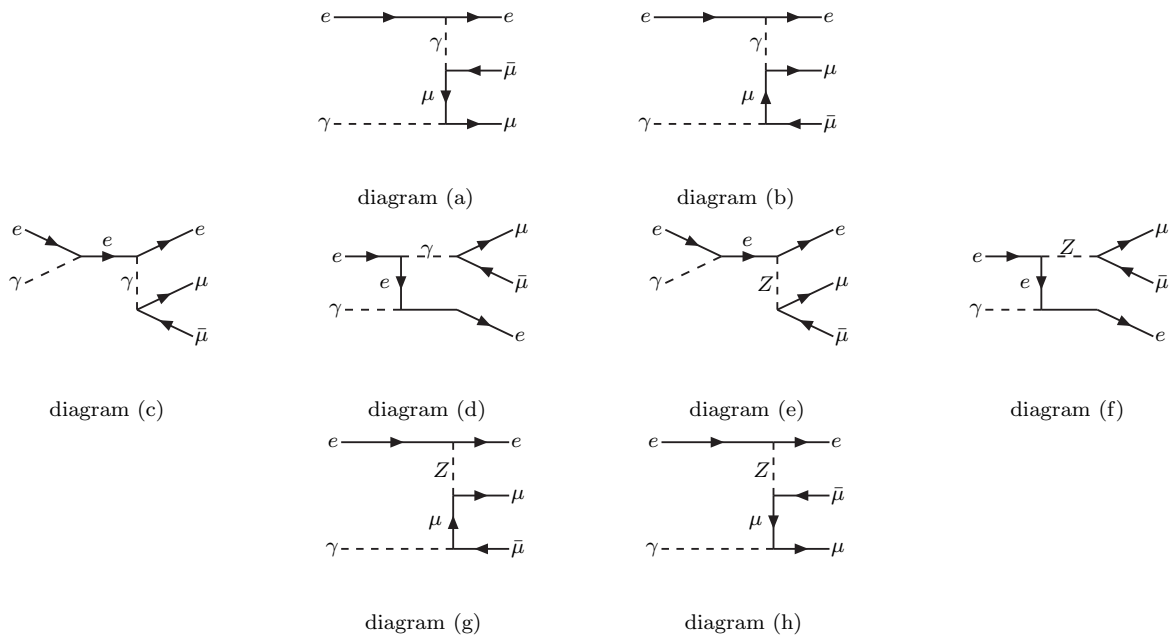

FIG. 1. The Feynman diagrams contributing to MPP in the leading order.

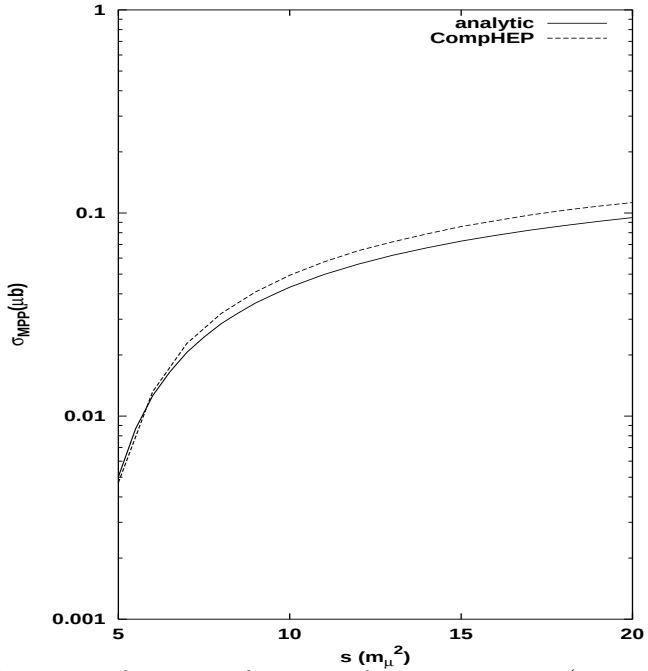

FIG. 2. σ_{MPP} as a function of square of center-of-mass energy s (in units of m_μ^2). Solid curve is obtained using Eq. (2). Dashed curve is obtained using CompHEP (it includes contribution from all 8 diagrams, see [6]).